Modeling of Growth using an Immersed Finite Element Method

Adnan Ebrahem[1,*], **René R. Hiemstra**[1], **Stein K. F. Stoter**[2], and **Dominik Schillinger**[1]

[1] Institute for Mechanics, Computational Mechanics, Technical University of Darmstadt, Germany

[2] Multiscale Engineering Fluid Dynamics Group, Eindhoven University of Technology, The Netherlands

To prevent remeshing, we explore the use of a non-boundary-fitted finite element method for the computational modeling of growth including contact mechanics. Accordingly, we utilize a mesh-related mapping procedure for the use of implicit geometry description by a level set function within the framework of immersed methods. Hence, our framework provides a setting to include patient-specific geometries based on imaging data as we use a level set function for the implicit geometry description. In this contribution, we show that the proposed approach is a viable alternative for problems with mesh-related obstacles, in particular when large growth simulations on complex patient-specific geometries are of primary interest.

1 Introduction

Over the last two decades, finite growth modeling has been widely studied for biological tissues [1–3]. Finite growth modeling has been mostly applied to biological tissues which are different from most engineering materials. Typical examples of volumetric growth are growing tumors [4], the heart [5], and the vascular tissue [6]. The main focus lies on the specification of individual growth laws for different types of tissues and on the identification of driving factors for growth in order to predict biological phenomena [1–6]. To our knowledge, computational modeling of growth is mainly embedded in a classical finite element framework, that operates in a boundary-fitted approach [1–9]. However, the fact that soft tissues undergo large deformations coupled with further difficulties in the human body, e.g. complex patient-specific, imaging data-based geometries or contact with surrounding organs, require remeshing within a classical boundary-fitted finite element approach.

Instead, we propose a approach to apply volume growth of solid bodies on a structured background mesh in an immersed boundary framework. The problem of remeshing is replaced by a problem of projection. The method is capable of incorporating large growth of solid bodies including contact mechanics without the necessity of remeshing. In the isotropic growth case the growing body is described by the deformations on the bounded boundary. Hence, we use a projection that maps the grown level set geometry back to the structured background mesh.

In general, it is not trivial to create analysis-suitable geometries or fitted finite element meshes for domains that are implicitly defined by a level set function such as imaging data-based geometries. In this context, our framework provides a setting to include imaging-based geometries.

2 Background and Notation

This section includes the continuum modeling within the framework of the finite growth theory, provides a brief review of immersed finite element methods and illustrates the concept of implicit geometry descriptions.

2.1 Finite growth mechanics

We start with the mathematical framework by considering the deformation map $\boldsymbol{\varphi}$. Material points $\boldsymbol{X}$ in the reference configuration Ω_0 at time $t = 0$ are mapped onto spatial points $\boldsymbol{x} = \boldsymbol{\varphi}(\boldsymbol{X}, t)$ in the deformed configuration Ω_t at any given time t. Within the framework of finite growth, the deformation map is decomposed into two steps. In the first step, a material point is mapped into an intermediate incompatible growth configuration Ω_g. This configuration is assumed to be stress-free as only mass generation occurs between Ω_0 and Ω_g. Next, elastic deformations are applied to the intermediate state to ensure the compatibility of the solid body [10]. This model results in a multiplicative decomposition of the deformation gradient

$$\boldsymbol{F} = \boldsymbol{F}_e \cdot \boldsymbol{F}_g \tag{1}$$

into a purely elastic part $\boldsymbol{F}_e$ and a growth deformation gradient $\boldsymbol{F}_g$ [10], which is analogous to the split of the deformation gradient in the theory of elastoplasticity, first introduced in [11] and afterwards applied to several material models.

A main task in finite growth is to define the growth deformation gradient

$$\boldsymbol{F}_g = \boldsymbol{F}_g(\vartheta, \boldsymbol{d}_0, \dots), \tag{2}$$

PAMM · Proc. Appl. Math. Mech. 2022;**22**:1 e202200183.   www.gamm-proceedings.com   **1 of 7**

https://doi.org/10.1002/pamm.202200183   © 2023 The Authors. *Proceedings in Applied Mathematics & Mechanics* published by Wiley-VCH GmbH.

which is a function of the growth ratio ϑ and possible or preferred directions $\boldsymbol{d}_0$ in which growth occurs. The growth ratio plays a key role in finite growth as it relates the stimuli of growth to the growth tensor which can be for example stress, nutrients or concentration driven. According to this, growth is usually governed by an evolution equation

$$\dot{\vartheta} = \dot{\vartheta}(\vartheta, \boldsymbol{C}, \boldsymbol{S}, \boldsymbol{d}_0, \dots), \tag{3}$$

where $\boldsymbol{C}$ is right Cauchy Green strain tensor and $\boldsymbol{S}$ is the second Piola-Kirchhoff stress tensor. Additionally, we include the mechanics by considering the balance of linear momentum

$$\rho_0 \dot{\boldsymbol{v}} = \mathrm{Div}(\boldsymbol{F} \cdot \boldsymbol{S}) + \rho_0 \boldsymbol{b}, \tag{4}$$

where $\boldsymbol{S} = 2\rho_0 \frac{\partial \psi}{\partial \boldsymbol{C}}$ denotes the second Piola-Kirchhoff stress tensor in the reference configuration, $\rho_0 \boldsymbol{b}$ is the momentum source with $\boldsymbol{b}$ being the body forces, ρ_0 is the density, $\boldsymbol{v} = \dot{\boldsymbol{\varphi}}$ is the spatial velocity and ψ describes the Helmholtz free energy. The elastic Piola-Kirchhoff stress can be obtained through a push forward to the intermediate configuration $\boldsymbol{S}_\mathrm{e} = \boldsymbol{F}_\mathrm{g} \cdot \boldsymbol{S} \cdot \boldsymbol{F}_\mathrm{g}^\mathrm{t}$.

2.2 Immersed finite element method

Immersed finite element methods, also known as unfitted or embedded domain methods, incorporate immersed geometries in non-boundary-fitted background meshes to solve boundary value problems (see Fig. 1).

In the framework of immersed methods, a physical domain Ω_phys of interest is extended with non-physical domain, also known as fictitious domain Ω_fict, to a larger domain of simple shape, referred to as the embedding domain [12]. Due to its simple shape, discretization appears on the embedding domain. We will refer to this as the structured background mesh.

Moreover, basis functions that are defined on the background mesh are only evaluated on the physical domain. In this context, there is no need of a boundary-fitted mesh. Instead the geometry of the physical domain is incorporated through integration of cut elements.

The main goal of immersed methods is to prevent mesh-related obstacles, e.g. remeshing and mesh distortion effects [13]. In addition to standard finite element technology, immersed methods require three basic components, which are (1) imposing Dirichlet boundary conditions at embedded surfaces utilizing penalty, Lagrange-multipliers or Nitsche-type methods [12] (2) a stabilizing mechanism for functions with small support and (3) evaluating surface and volume integrals in cut elements. Therefore, geometrically faithful quadrature plays a major role.

For example, the finite cell method uses an adaptive quadrature technique for all cut elements by recursive quadtree subdivision in 2D and octree subdivision in 3D. Alternative strategies to integrate cut elements are parametrization techniques, which ensure optimal accuracy and rely on mappings to enable geometrically accurate parametrization of cut elements [14]. Within this work, we make solely use of the higher-order accurate quadrature algorithms for implicitly defined domains described in [15] which can be used to solve surface or volume integrals of a geometry intersecting an element. For details on the used quadrature algorithms, we refer the interested reader to [15].

2.3 Implicit geometry

The domain boundary Γ of an implicit geometry in an Euclidean space is characterized as the zero contour of a function ϕ by

$$\Gamma = \{\boldsymbol{x} | \phi(\boldsymbol{x}) = 0\}, \tag{5}$$

often referred to as a level-set height function [16]. A signed distance function outputs the orthogonal distance of a given point $\boldsymbol{x}$ to the boundary Γ of a domain and satisfies the condition

$$|\nabla \phi| = 1. \tag{6}$$

The sign of the function determines the position of the point $\boldsymbol{x}$. Inside the domain Ω the function ϕ takes positive values while outside it is negative, such that

$$\Omega^+ = \{\boldsymbol{x} | \phi(\boldsymbol{x}) > 0\}, \tag{7}$$
$$\Omega^- = \{\boldsymbol{x} | \phi(\boldsymbol{x}) < 0\}. \tag{8}$$

3 Computational aspects of immersed growth with contact

In this section, we present the basic components of the proposed approach for the computational modeling of volumetric growth within an immersed setting.
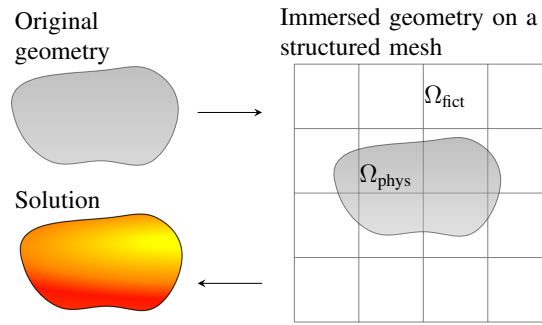
Fig. 1: Concept of immersed methods. Immersed discretization of an embedded physical domain Ω_phys extended with a fictitious domain Ω_fict.

3.1 Implicit level set geometry

We introduce a level set based geometry description, whose domain boundary is characterized by a zero value, using basis functions. The level set height function is defined as

$$f(\boldsymbol{x}) = \sum_{i=1}^{n} N_{i,p}(\boldsymbol{x})C_i, \tag{9}$$

in which $\boldsymbol{C} \in \mathbb{R}^n$ denote the level set coefficients and $N_{i,p}$ are the n basis functions of degree p of a continuous finite element space [17].

We approximate a given geometry by computing the coefficients C_i of the level set height function $f(\boldsymbol{x})$. We define the level set coefficients as

$$C_i = \frac{\int_{\Omega_\text{El}} N_{i,p}(\boldsymbol{x})g(\boldsymbol{x})\mathrm{d}\boldsymbol{x}}{\int_{\Omega_\text{El}} N_{i,p}(\boldsymbol{x})\mathrm{d}\boldsymbol{x}}, \tag{10}$$

where g originates from approaches of scan based geometry description and denotes the gray scale function $g : \Omega_\text{scan} \to \mathbb{R}$ which contains the gray scale values $\boldsymbol{a} \in \mathbb{R}^{\text{no}_\text{vox}}$ in the voxels with no_vox being the number of voxels [17]. Ω_El corresponds to the element domain. The voxel-based geometry can be extracted from the gray scale data and is linked to a much coarser background mesh.

Each element satisfy the partition of unity property and no mean value occurs zero over an element. The equation (10) is a low order approximation, so the approximation of the level set function will converge only linearly independent of the polynomial order of the basis. Furthermore, Gibb's type effects are a consequence of least square approximations and not a consequence of the higher order case [18]. As described in [17], equation (10) satisfies properties which ensures that no Gibb's type effects arise. For more details we refer the interested reader to [17].

3.2 Geometry mapping

The argumentation in the introduction motivates the use of a mesh-related geometry mapping within the framework of the immersed finite element method. The schematic representation for the mapping procedure of the grown geometry can be seen in Fig. 2. The starting point is the L^2 projection, which mathematically can be formulated as a minimisation problem. Find $f_\text{new} \in V_\text{h}$ so that

$$\int_\Omega f_\text{new} v \, \mathrm{d}\Omega = \int_\Omega f_\text{old} v \, \mathrm{d}\Omega \ \ \forall v \in V_\text{h}, \tag{11}$$

where

$$f_\text{new} \in V_\text{h} \subset H^1(\Omega), \tag{12}$$

$$v \in V_\text{h} \subset H^1(\Omega), \tag{13}$$

$$f_\text{old} \in \hat{V}_\text{h} \subset H^1(\hat{\Omega}). \tag{14}$$

The function f_old describes the level set function on the deformed domain $\hat{\Omega} \subset \mathbb{R}^n$, f_new denotes the mapped level set function on the undeformed domain $\Omega \subset \mathbb{R}^n$ and v are the test functions on the undeformed domain Ω. The representation of both level set functions differs through the basis functions defined on different domains. The only challenge is to evaluate the old level set function in the undeformed domain, so

$$f_\text{old} = f_\text{old}(x), \ \ x \in \Omega. \tag{15}$$
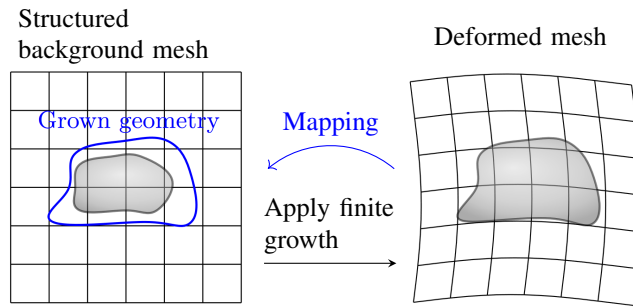
Fig. 2: Schematic representation of finite growth and subsequent mapping procedure of grown geometry in the framework of the immersed method. Grown geometry on structured mesh after projection is depicted in blue.

This approach can also generally be used for immersed methods where large deformations leads to increased levels of mesh distortion unrelated to finite growth.

4   Numerical benchmarks

Two examples are presented in the following to demonstrate finite growth analysis with contact mechanics in the immersed framework. The immersed finite element method and the contact problem are implemented in the Julia programming language. In order to perform numerical integration of cut elements and apply the quadrature algorithms described in [15] we make use of the C++ library Algoim [21] and embed it in Julia.

The first example is the isotropic growth of a sphere for which the analytical solution of the deformations

$$u^3 = 3 \int_0^r \Theta^3(\tilde{r})\tilde{r}^2 \mathrm{d}\tilde{r} \tag{16}$$

exists, where u is the displacement field, Θ is in the non-constant case a function of the radius and r corresponds to the radial coordinate [19]. In the case of isotropic growth, we follow [20] and define the isotropic growth tensor as

$$\boldsymbol{F}_{\mathrm{g}} = \vartheta \boldsymbol{I}, \tag{17}$$

with $\boldsymbol{I}$ being the identity tensor. We apply the previously described finite growth equations and the function

$$\Theta = \vartheta - \tilde{r} = 0.3\tilde{r} \tag{18}$$

with the growth function $\vartheta = 1.3\tilde{r}$ which depends on the radius of the sphere. We compute the growth of the sphere within the immersed framework and apply a quasi-static setting ($\dot{\boldsymbol{v}} = \boldsymbol{0}$) and no body forces ($\boldsymbol{b} = \boldsymbol{0}$). Additionally, we use a hyperelastic material model by utilizing a free energy density ψ of Neo-Hookean type which can be expressed in terms of the first and third invariant of the elastic right Cauchy Green tensor

$$\psi = \frac{1}{8}\lambda \ln^2(I_3) + \frac{1}{2}\mu[I_1 - 3 - \ln(I_3)], \tag{19}$$

where $I_1 = \mathrm{tr}(\boldsymbol{C}_{\mathrm{e}})$, $I_3 = \det(\boldsymbol{C}_{\mathrm{e}})$, $\boldsymbol{C}_{\mathrm{e}} = \boldsymbol{F}_{\mathrm{e}}^{\mathrm{t}} \cdot \boldsymbol{F}_{\mathrm{e}}$ and λ and μ describe the Lamé coefficients [6]. To compute the level set function in the benchmark, we use the function g from equation (10) as a function to perform inside/outside test by checking whether Gauss points are inside or outside the domain and define the function g as

$$g(\boldsymbol{x}) = \begin{cases} 1 & \boldsymbol{x} \in \Omega_{\mathrm{phys}} \\ -1 & \boldsymbol{x} \in \Omega_{\mathrm{fict}}. \end{cases} \tag{20}$$

For the actual analysis we compute the growth solution field of an eighth of a sphere due to symmetry conditions (see Fig. 3) and compare the numerical results with the analytical solution.

In the case of using the definition (10) of the level set height function we obtain suboptimal convergence if we compute the L^2 norm in terms of the deformation field (Fig. 4 (a)) which is justifiable for the case when we work with imaging data and contact of soft tissues as higher order accuracy can not be expected.

Another possibility to compute the level set coefficients is via a signed distance function ϕ. In this case, the signed distance function for a sphere is given by

$$\phi = R - \sqrt{x^2 + y^2 + z^2}. \tag{21}$$
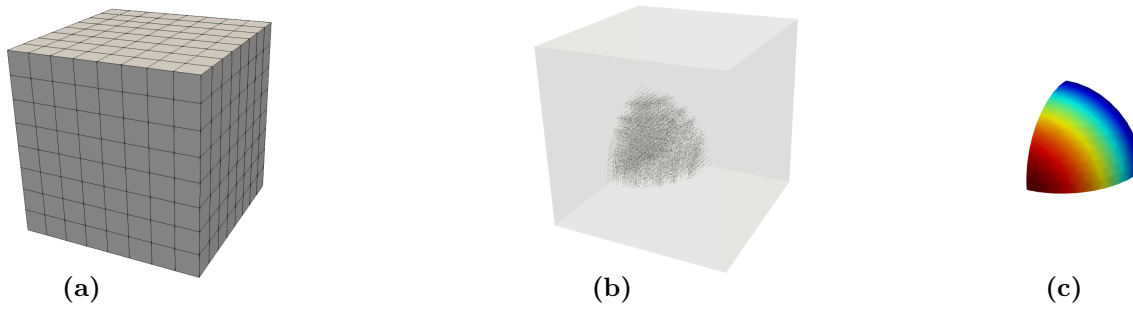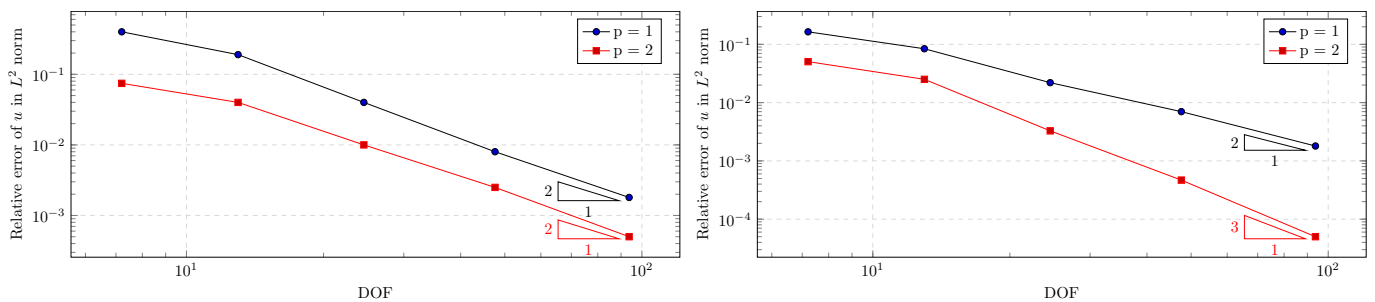
Fig. 3: Finite growth within immersed method. **(a)** Background mesh consisting of $8 \times 8 \times 8$ linear elements, **(b)** Gauss points representing geometry and **(c)** Growth plotted on deformed configuration.

(a) Application of equations (9) and (10) for implicit geometry.

(b) Application of equations (9) and (22) for implicit geometry.

Fig. 4: Convergence of the error in the L^2 norm for displacement u. Level set functions are applied for geometry description. Numerical results of displacement field are compared to analytical solution in equation (16).

As we use a nodal-interpolatory approach, we can directly extract the coefficients from

$$C_i = R - \sqrt{x_i^2 + y_i^2 + z_i^2}, \tag{22}$$

where R is the radius of the sphere and $\{x_i, y_i, z_i\}$ are the coordinates of the nodal point i. As can be seen in Fig. 4 (b), we obtain optimal convergence if we apply the coefficients in equation (22) extracted from a signed distance approach.

However, the advantage of using equation (10) instead of equation (22) lies in the fact that it is compatible with imaging data. In future work, we will use equation (10) and apply linear basis function to model growth of patient-specific imaged-based human liver experiencing contact with surrounding organs.

Additionally, we briefly introduce the treatment of frictionless contact as contact possibly occurs in the growth modeling of soft tissues. We apply the penalty method [22] for contact which benefits from various advantages like no additional unknowns, symmetry and positive definiteness of the stiffness matrix. The penalty method is based on including an additional penalty term δW_p to the weak form of the underlying problem. The penalty term, which is obtained by integration over the Contact boundary $\partial \mathcal{S}^c$, can be expressed as

$$\delta W_p(\boldsymbol{u}, \delta \boldsymbol{u}) = \beta \int_{\partial \mathcal{S}^c} \boldsymbol{g}(\boldsymbol{u}) \cdot \delta \boldsymbol{u} \mathrm{dA} \tag{23}$$

where β describes the scalar penalty parameter and $\delta \boldsymbol{u}$ are the test functions. The vector $\boldsymbol{g} = \boldsymbol{u} - \hat{\boldsymbol{u}}$ is the penetration in which $\boldsymbol{u}$ are the unknown displacement and $\hat{\boldsymbol{u}}$ denote the displacement on $\partial \mathcal{S}^c$.

Thus, the next benchmark consists of a growing sphere that experiences contact within the immersed framework. We compute a sphere that grows against a rigid plane (see Fig. 5). The numerical efficiency of the contact formulation in the immersed framework is evaluated by confirming the convergence of the Newton scheme which converges in 5 iterations to a residual norm of 10^{-6}.

5   Summary and conclusion

In this work, we present a non-boundary-fitted finite element method for growth modeling including contact mechanics and a mapping procedure for implicit level set geometry descriptions. The numerical efficiency of the method is evaluated by
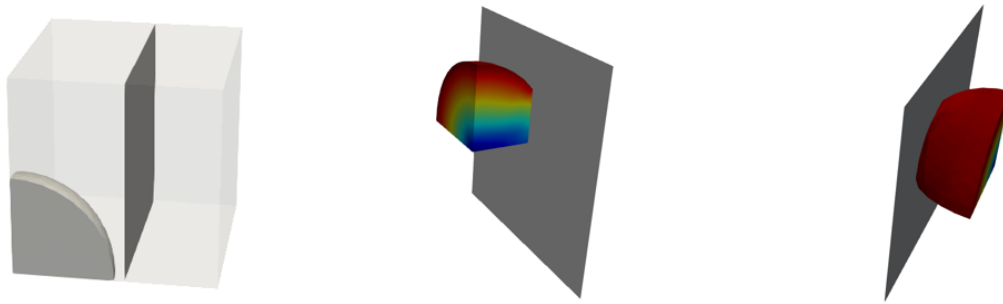
Fig. 5: Unilateral contact of a sphere within immersed framework

confirming the convergence behaviour for a three-dimensional numerical benchmark. As an outlook to future work, we will apply this approach to a biomedical patient-specific problem, where we will focus on modeling the regrowth of the human liver. The aim is to make use of the mapping scheme and compute large growth ratios without the need of remeshing. The modeling goals are to investigate how residual stresses develop during liver size regeneration, how they are distributed and which influence they have on the growth directions of the liver.

References

[1] Ambrosi D, Ateshian GA, Arruda EM, Cowin SC, Dumais J, Goriely A, Holzapfel GA, Humphrey JD, Kemkemer R, Kuhl E, Olberding JE, Taber LA, Garikipati K (2011) Perspectives on biological growth and remodeling. J Mech Phys Solids **59**:863-883

[2] Menzel A, Kuhl E (2012) Frontiers in growth and remodeling. Mech Res Commun **42**:1-14

[3] Göktepe S, Acharya SNS, Wong J, Kuhl E (2011) Computational modeling of passive myocardium. Int J Numer Methods Biomed Eng **27**:1-12

[4] Ambrosi D, Mollica F (2002) On the mechanics of a growing tumor. Int J Eng Sci **40**:1297–1316

[5] Kroon W, Delhaas T, Arts T, Bovendeerd P (2009) Computational modeling of volumetric soft tissue growth: application to the cardiac left ventricle. Biomech Model Mechanobio **8**:309–310

[6] Kuhl E, Maas R, Himpel G, Menzel A (2007) Computational modeling of arterial wall growth. Biomechan Model Mechanobiol **6**:321–331

[7] Göktepe S, Abilez OJ, Kuhl E (2010) A generic approach towards finite growth with examples of athlete's heart, cardiac dilation, and cardiac wall thickening. J Mech Phys Solids **58**:1661-1680

[8] Kuhl E (2014) Growing matter: A review of growth in living systems. J Mech Behav Biomed Mater **29**:529-543

[9] Himpel G, Kuhl E, Menzel A, Steinmann P (2005) Computational modelling of isotropic multiplicative growth. Comp Mod Eng Sci **8**:119–134

[10] Rodriguez EK, Hoger A, Mc Culloch AD (1994) Stress-dependent finite growth in soft elastic tissues. J Biomech **27**:455-467

[11] Lee EH (1969) Elastic-plastic deformation at finite strains. J Appl Mech **36**:1–6

[12] Schillinger D, Ruess M, Zander N, Bazilevs Y, Düster A, Rank E (2012) Small and large deformation analysis with the p-and B-spline versions of the finite cell method. Comput Mech **50**:445–478

[13] Parvizian J, Düster A, Rank E (2012) Topology optimization using the finite cell method. Optim Eng **13**:57–78

[14] Lehrenfeld C (2016) High order unfitted finite element methods on level set domains using isoparametric mappings. Comput Methods Appl Mech Engrg **300**:716–733

[15] Saye RI (2015) High-order quadrature methods for implicitly defined surfaces and volumes in hyperrectangles. SIAM J Sci Comput **37**:A993-A1019

[16] Osher S, Sethian JA (1988) Fronts propagating with curvature-dependent speed: Algorithms based on Hamilton-Jacobi formulations. J Comput Phys **79**:12-49

[17] Verhoosel CV, van Zwieten GJ, van Rietbergen B, de Borst R (2015) Image-based goal-oriented adaptive isogeometric analysis with application to the micro-mechanical modeling of trabecular bone. Comput Methods Appl Mech Engrg **284**:138–164

[18] Foster J, Richards FB (1991) The Gibbs Phenomenon for Piecewise-Linear Approximation. Am Math Mon **98:1**, 47-49

[19] Alain Goriely, The Mathematics and Mechanics of Biological Growth, Volume 45 (Springer, New York, 2017), p. 435.

PAMM · Proc. Appl. Math. Mech. **22**:1 (2022)

7 of 7

[20] Lubarda VA, Hoger A (2002) On the mechanics of solids with a growing mass. Int J Solids Struct **39**:4627–4664

[21] Saye R, Algoim: Algorithms for implicitly defined geometry, level set methods, and Voronoi implicit interface methods. Lawrence Berkeley National Laboratory. https://algoim.github.io/

[22] Peter Wriggers, Computational Contact Mechanics, Second Edition (Springer, Berlin Heidelberg, 2006), p. 118.